EPJ D
Atomic, Molecular, Optical and Plasma Physics
EPJ.org
your physics journal

Eur. Phys. J. D (2017) 71: 180 DOI: 10.1140/epjd/e2017-80051-8

Hierarchy effect on electronic structure and core-to-valence transitions in bone tissue: perspectives in medical nanodiagnostics of mineralized bone

Dmitrii O. Samoilenko, Alexander S. Avrunin and Andrey A. Pavlychev

edp sciences
Società Italiana di Fisica
Springer

Eur. Phys. J. D (2017) 71: 180
DOI: 10.1140/epjd/e2017-80051-8

THE EUROPEAN PHYSICAL JOURNAL D

Regular Article

Hierarchy effect on electronic structure and core-to-valence transitions in bone tissue: perspectives in medical nanodiagnostics of mineralized bone*

Dmitrii O. Samoilenko[1,a], Alexander S. Avrunin[2], and Andrey A. Pavlychev[1]

[1] Solid State Electronics Department, St-Petersburg State University, St. Petersburg, 198504, Russia
[2] Vreden Russian Research Institute of Traumatology and Orthopedics, St. Petersburg, 195427, Russia

Received 25 January 2017
Published online 4 July 2017 –

Abstract. Electronic structure and core-to-valence transitions in bone tissue are examined in the framework of the morphological 3DSL model that takes into account (i) structural and functional organization of the skeleton in the normal and pathological conditions and (ii) peculiarities of electron wave propagation in a three-dimensional superlattice of "black-nanocrystallites-in-muddy-waters". Our focus is on the HAP-to-bone red shifts of core-to-valence transitions near Ca and P $2p$ and O $1s$ edges in single-crystal hydroxyapatite (HAP) $Ca_{10}(PO_4)_6(OH)_2$. The origin of the HAP-to-bone shift is discussed and the extended comparative analysis of the experimental data is performed. The detected spectral shift is assigned with the effect of hierarchical organization of bone tissue. This hierarchy effect on the core-to-valence transition energies is regarded as a promising tool for medical imaging and perspective pathway for nanodiagnostics of mineralized bone.

1 Introduction

In modern medicine, the problems originated from bone and bone and joint pathology are of great socio-economic importance associated primarily with economic costs directed to medical treatment, rehabilitation and care of patients with osteoarthritis and the consequences of osteoporosis. As an example, osteoarthritis is the fourth most common cause of hospitalization. Annual costs, according to various estimates range from 3.4 up to $60 billion, which is associated only with medical care (51%) and a decrease in productivity (49%) [1].

Bone is the most intriguing hierarchically organized, nano- and mesostructured material in nature. The morphological models [2–9] based on ideas concerning the structural and functional organization of the skeleton in the normal and pathological conditions describe peculiarities of skeletal structural organization and its functional properties. Unfortunately, the descriptive character of these models makes it difficult to use them for quantitative study of mechanical, physical, chemical and osteochondral processes in the skeleton. Elaboration of quantitative ex- and in-vivo models of bone tissue and their comprehensive verification by applying new experimental techniques is a key problem for medicine and medical materials science. The models have evidently to take into account relationships between the electronic and atomic structure and the hierarchical organization of bone tissue.

X-ray spectroscopy is a prospective pathway to extract quantitative information about nanocomponents and develop novel methods of medical imaging and nanodiagnostics of bone tissue. In addition to these prospects the investigations of atomic and molecular architecture of bone will enable us to determine optimal conditions for its self-healing. Apart of the medical goals the nanoscopy of the hierarchical nanostructures favors for developing of both cutting-edge nanotechnologies and for bio-designing of advanced materials [9].

There are two morphological concepts of hierarchical organization of bone tissue. One of them considers the structural and functional organization of the skeleton in the normal and pathological conditions excluding the organic component of the skeleton. The other takes into account relationships of the mineralized and organic hierarchical structures [5–7]. In addition to the hard hydroxyapatite (HAP) mineral and the flexible collagen molecules there exists the third important component of the mineralized bone, which is water. It is observed in both inter and intracrystallite states [10–14].These concepts hardly describe the water role in the hierarchical organization.

Recently the quantitative 3DSL model of bone tissue is suggested [15]. It takes into account (i) structural and functional organization of the skeleton in the normal and pathological conditions and (ii) peculiarities of electron

* Contribution to the Topical Issue "Dynamics of Systems at the Nanoscale", edited by Andrey Solov'yov and Andrei Korol.

[a] e-mail: dmitri.samoilenko@yandex.ru

wave propagation in a three-dimensional superlattice of "black-nanocrystallites-in-muddy-waters". The mineralized bone is regarded as multilevel hierarchically organized structure. Its first (lowest) level is three-dimensional atomic structure of the single-crystal $Ca_{10}(PO_4)_6(OH)_2$ HAP; the coplanar assemblies of nanocrystallites of HAP (NHAP) are attributed to the second level. The NHAP separated one from the other by the hydrated nanolayers form the mineralized plates that reproduce the helix shape of the collagen molecules. These plates are regarded as the third (mesoscopic) level [15]. Further associations into macroscopic complexes within each bone are assigned with the higher hierarchical levels [8]. The assemblies of NHAP are located either in intra- or interfibrillar positions in the bone tissue. According to the experimental data [5] far from the collagen fibrils the nanocrystallites are oriented practically in the same direction.

Our attention here is attracted to spectral changes in core-to-valence transitions near the Ca $2p$, P $2p$ and O $1s$ edges in native bone. That can help to understand and visualize the effect of its hierarchical organization on its local electronic states. We keep our emphasis on electronic and atomic structure of the mineralized phase, as collagen being the main structural protein is studied in more detail (see, e.g. [6,16]).

2 The hierarchy effect

The electronic and atomic structure of the perfect-crystal HAP is well studied [17,18]. The band theory describes the mineral as insulator with the gap ≈5 eV. The bonding studies indicate that HAP is determined by the sets of nearly tetrahedral anions $[PO_4]^{3-}$ and Ca^{2+} channels populated by columns of OH^- anions [7]. Strong ionic conductivity of HAP is attributed to high mobility of hydroxyl. Considering the electronic and atomic structure of the single-crystal HAP as a background level we bring out the main structural peculiarities inherent to native bones and link the lowest hierarchical level with the upper ones. The mechanisms linking the hierarchical levels attract our attention.

Both electron transmission microscopy and small angle X-ray scattering make evident that intra- and interfibrillar associations of the NHAP form a series of parallel and spiral wound mineralized plates [5,6,19]. They are usually considered as coplanar assemblies of the NHAP [5,19]. The fragment $(3 \times 3 \times 3)$ of such assembly is plotted in Figure 1. The individual nanocrystallites are separated by nanolayers of saturated aqueous solution containing the ions OH^-, $[PO_4]^{3-}$ and $[CO_3]^{2-}$ and Ca^{2+}.

It is also known that size distribution of the NHAP in the mineralized bone is an age-related function [6,20,21] and depends on atomic incorporations and substitutions [22,23]. To date, many efforts have been invested to investigation of the influence of chemical composition on electronic properties of bioapatite in bone tissue. Recently it was shown [15] that the near edge X-ray absorption fine structure (NEXAFS) spectroscopy provides a sensitive probe of local electronic structure and its dependence on hierarchical organization of bone tissue.

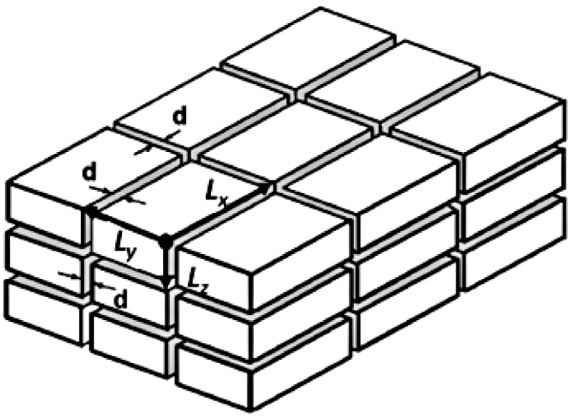

Fig. 1. The fragment $(3 \times 3 \times 3)$ of a coplanar assembly of NHAP is schematically presented. The uniform and equal size $(L_x \times L_y \times L_z)$ NHAP are separated one from the others by the hydrated layers. d denotes their thickness.

The mineralized plate in bone is described as a 3D-superlattice assembled from the equal dielectric nanocrystallites separated by the uniform nanolayers. Using the average sizes of the NHAP $\langle L_j \rangle$ and the hydrated layers $\langle d \rangle$ the basic vectors of translation $\mathbf{a_j} = \mathbf{L_j} + d$ of the superlattice are determined as ≈22.0, 9.5 and 5.5 nm, where $\mathbf{L_j} = L_j \boldsymbol{j}$ and $\boldsymbol{j}$ is the unit vector in Cartesian coordinates. These basic vectors are marked in Figure 1. The individual NHAP is collected from the crystallographic cells of HAP as it is shown in Figure 2. To simplify the assembly the extended crystallographic cell taken as a rectangular parallelepiped $16.4 \times 9.43 \times 6.98$ Å^3 is used [15]. This expansion is based on the conventional crystallographic cell that has a dihedral angle of 120° with an edge of 6.98 Å. Then we add the adjacent cell and cut them to get a parallelepiped allowing us to reproduce the hexagonal lattice of HAP. From the model geometry of the NHAP follows that there are about 4×10^4 atoms per crystallite and the volume shares of the mineral phase and the hydrated layers are 46% and 54% in the coplanar assembly.

The NHAP is assembled in such a way to provide coincidence of their coplanar assembly with the perfect-crystal HAP in case the hydrated layers disappear. This means that the electronic structure of the coplanar assembly will approach to the band structure of perfect HAP when $d \to 0$. Considering the NHAP as a quantum dot we obtain the orthorhombic superlattice. The cyclic border conditions are applied to describe the electronic structures of the individual NHAP and their coplanar assembly [15]. Since the mineralized phase is conventionally regarded as a nanostructured HAP with low crystallinity [4,24] and the hydrated layers are disordered the pseudopotential 3DSL of "black-nanoboxes-in-muddy-waters" model is a promising way to understand the hierarchy effect on core-to-valence transitions in HAP [15].

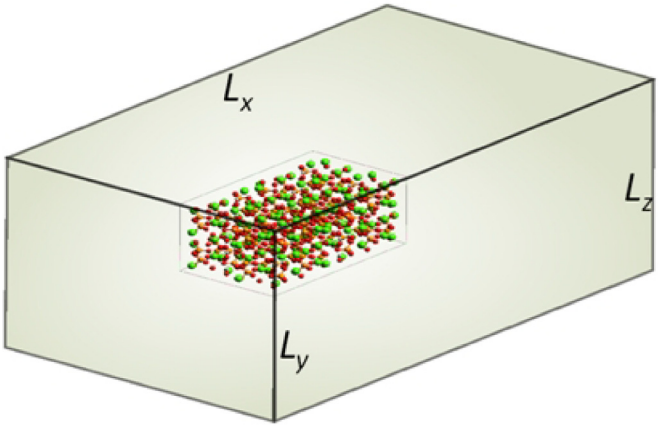

Fig. 2. The individual NHAP presented schematically as an extended crystallographic HAP cell. Calcium, phosphorous and oxygen atoms in the crystallite are labeled on-line as green, orange and red circles, respectively.

The hierarchy effect on electronic structure and core-to-valence transitions in the coplanar assemblies is closely related with the size of NHAP. In the framework of the 3DSL model the dispersion $E(k)$ of electronic states in the coplanar assembly is a function of $\langle d\rangle$ and $\langle L\rangle$ can be investigated by using Heine equation [15,25]

$$e^{2i\mathbf{ka}} - 2\mathrm{Re}\left(\frac{1}{T(E;\langle d\rangle,\langle L\rangle)}\right)e^{2i\mathbf{ka}} + 1 = 0 \qquad (1)$$

In general, Heine equation links the electronic structure of a periodic system (with the basic vectors $\mathbf{a}$) with the amplitude (T) of electron transmission through its cell and assigns the certain energy E to the electron wave vector $\mathbf{k}$ [25]. The amplitude $T(E;\langle d\rangle,\langle L\rangle)$ is determined by interference of the incident electron wave and waves scattered on atoms belonging to the cell and depends on the amplitudes T' and T'' of the waves transmitted (forward scattered) through and the amplitudes B' and B'' reflected (back scattered) from the NHAP and the hydrated layer respectively. Taking the results [26] into account we derive

$$\mathrm{Re}\left(\frac{1}{T}\right)_j \approx \mathrm{Re}\left|\left(\frac{1 - B'B''\exp(-4ikL)}{T'T''}\right)_j\right| \times \cos(k(d + L_j) + \Theta_j) \qquad (2)$$

$\Theta = \arg(\mathrm{Re}T^{-1})$. The solution of equation (1) can be simplified in assumption that the multiple scattering of the backscattered waves is negligibly weak, i.e.

$$|B'B''| \ll 1 \qquad (3)$$

Then, the second term on the left side of equation (1) can be rewritten as

$$\mathrm{Re}\left(\frac{1}{T}\right)_j \approx \left|\frac{1}{T'_j(\kappa)T''_j(\kappa)}\right|\cos(\kappa a_j + \tau_j + \gamma) \qquad (4)$$

Equation (4) coincides with that obtained in [15]. $\kappa = \sqrt{E}$, τ and γ are respectively the electron scattering phase shifts on the potentials of NHAP and hydrated layer taken separately. In case the condition (3) is invalid the resonant features in interface of NHAP and hydrated layers are expected to influence on electronic structure of bone tissue. In particular, the features similar to the transparency windows [26] are expected to appear.

Analyzing equation (4) the HAP-to-bone red shift δE_n [15] of electronic bands and core-to-valence transitions can be predicted

$$E^{(n)}_{assembly} - E^{(n)} \equiv \delta E_n \approx E^{(n)}\frac{\tilde{d}}{\langle L\rangle} \qquad (5)$$

$E^{(n)}$ and $E^{(n)}_{assembly}$ are energies of n-band in the single crystal HAP and the corresponding state in coplanar assembly of NHAP, $\tilde{d}$ is the electron-optical length of the separating layer and $\langle L\rangle$ is the average size of the NHAP. According to the 3DSL model, the shift δE_n is originated by the super periodicity of the coplanar assembly and demonstrates linear dependence on both the band energy in the single-crystal and the ratio of the thickness of the spacer layers to the size of the nanocrystallite. Within these approximations the red shift δE_n can be attributed to the comprehensive expansion of the assembly as compared with the single crystal due to the incorporation of the spacer layers. Considering the NHAP as a specific quantum dot we infer that the energy position of a quantum state in it drops with a decrease of its radius. In particular, for the Ca $3d-$ and P $\epsilon d-$ bands in HAP the geometric partition of the perfect crystal leads to the red shift

$$\delta E_{\mathrm{Ca}3d} \approx 0.4 \text{ eV} \quad \text{and} \quad \delta E_{\mathrm{P}\epsilon d} \approx 3 \text{ eV}$$

In addition to the shift, the narrowing of the core-to-valence bands in X-ray absorption spectra of native bone is also expected. Since the size distribution of NHAP and their mean size are age-related functions [27,28] the shift controls the hierarchy effect on the band structure of HAP and can be attributed to *HAP-to-bone* shift. The geometric ratio $\frac{\tilde{d}}{\langle L\rangle}$ in equation (5) is maximal for young bone and drops for mature one [29]. Thus, one can speak about the hierarchy-induced size-dependent phenomena in both electronic structure and core-to-valence transitions in bone tissue. We note that age-related changes of the hydrated layer thickness are less studied.

3 Experimental data analysis

To visualize the hierarchy effects on electronic structure, the high resolution near Ca and P $2p$ and O $1s$ edges X-ray absorption fine structure (NEXAFS) of bone tissue measured in the works [15,30,31]. NEXAFS of native bone are examined and compared with the X-ray absorption spectra of reference compounds to check the hierarchy effects on electronic structure of native bone. Specifically the interplay of short-, long- and super-range order parameters in mineralized bone tissue makes evident the distinct

Table 1. The red shifts of the core-to valence transitions in bone tissue in comparison with references objects. The transition energies in the references are taken for zero (cols. 2 and 5). The shifts are measured in eV. The symbols *, ⋆, **, •, mark respectively the results of the works [15,30–33].

HAP-to-bone and aqua-solution-to-bone red shifts of the core-to-valence transitions	HAP⋆	Native bone*	Heated bone, $T = 400^{\star}$	Aqua solution of KOH(NaOH)•
Ca $L_3(2p_{3/2}) \rightarrow 3d$	0	0.6 (0.2)**	≈0	×
Ca $L_3(2p_{1/2}) \rightarrow 3d$	0	0.6 (0.2)**	≈0	×
P $L_3(2p_{3/2}) \rightarrow a_1(3s)$	0	1.5 (2.2)**	≈0.2	×
P $L_{2,3}(2p_{1/2,3/2}) \rightarrow t_2(\epsilon d)$	0	3.1 (2.2)**	≈0.1	×
O $K(1s) \rightarrow LUMO$	×	0.3 (0.6)	×	0

spectral changes in electronic structure of the mineralized phase compared with the single-crystal HAP. It is shown that the *HAP-to-bone* red shift is a product of the band energy in HAP and the geometric ratio of the thickness of the separated layer to the linear size of the NHAP. In the framework of the 3DSL model the electronic structure of the mineralized phase is approaching to the band structure of the single-crystal HAP and the *HAP-to-bone* red shifts disappear when the geometric ratio comes to nil.

The experimental *HAP-to-bone* as well as *aqua-solution-to-bone* red shifts are collected in Table 1. The core-to-valence transition energies from Ca and P $2p$ levels in HAP are regarded as reference values. They are taken equal to zero in Table 1. The transition energies in aqua solution of KOH (NaOH) for O $1s$ level are also taken as references for determination of the *aqua-solution-to-bone* red shifts. They refer to the O $1s$-to-LUMO transition in native bone relative to the energy position of A-line (see discussion in [15]) in the aqua solutions [32,33].

Two sets of experimental the *HAP-to-bone* shifts of Ca $L_3(2p_{3/2,1/2}) \rightarrow 3d$ [15,31] confirm the hierarchy effect on the core-to valence transition in calcium cation and support the estimated red shift ≈0.4 eV derived from equation (4). Their deviation could be related with different hierarchical organization of the fish [31] and rat [15] bone tissues. We note that the measured shift of the white lines [31] is detected at the same experimental conditions providing direct evidence of the predicted hierarchy induced spectral shift. We also pay our attention to the fact that the energies of the Ca $L_3(2p_{3/2,1/2}) \rightarrow 3d$ transitions in HAP, Ca_3PO_4 and $CaCO_3$ do not show any visible shifts. The observed increase of the *HAP-to-bone* shifts of the P $L_{2,3}(2p_{1/2,3/2})$ transitions is in good agreement with the 3DSL-model expectations (3 eV). Since the intense O $1s \rightarrow LUMO$ transition in native bone disappears in heated bone it is attributed to oxygen atoms associated with intercrystallite water located in the hydrated layers. On this basis spectral distribution of oscillator strength for this transition in native bone could be assigned with O 1s transitions in molecular-like fragments such as $OH^-(H_2O)_m$, $Ca^{2+}(H_2O)_n$, carboxyl, $[PO_4]^{2-}$, $[PO_4]^-$ [15].

We note that the bone samples are prepared from different animals and different techniques are applied. In the work [15] the powdered and sliced bone samples are derived from cortical middle third of the femur, tibia and humerus white mongrel male rats weighing 180–220 g. Cortex has been cleaned of soft tissue, washed in saline and dried with blotting paper. In the work [31] the bone samples are obtained from ice fishes. Fish bones were collected after 2-week long preliminary cleaning with maggots and were washed using distilled water. After drying on air the bones are placed in a 15% aqueous solution of NaOH for 30 min at room temperature and washed with distilled water to remove lipids followed by treatment using 6% solution of H_2O_2. In the both studies the XANES is detected by measuring the total electron yield. In the work [30] the P $2p$ transition energies in the powdered bone of sheep are measured by using X-ray fluorescence yield. The spectral resolutions of the presented data are expected to be comparable for the Ca and P $2p$ and O $1s$ regimes respectively. Considering the absolute energy calibration of the core-to-valence transitions we see that it is nearly the same in the works [15] and [31] but differs from that of in [30]. This peculiarity is an additional source of the deviations in the red shifts under study.

In contrast to the *HAP-to-bone* red shift the relevant shift of core-to valence transitions in defect centers in bioapatite in bone tissue is not expected because these centers do not form the superlattice of the NHAP. The effect of the mineral - protein superperiodicity is not discussed here as being of higher hierarchical level.

4 Conclusion

Summarizing the study we note that the 3DSL model gives us a key for understanding relationships between hierarchical organization of bone tissue and the local electronic structure of the mineralized phase and spectral distribution of oscillator strength for core-to-valence transitions in it. In addition to the complicated elemental composition of bioapatite, the size distribution of the nanocrystallites in mineralized bone influences its electronic structure and opens the way to functionalize its chemical and physical properties. Fine tuning of ion exchange processes needs further theoretical and experimental investigations of the hierarchy-induced changes in electronic structure. X-ray absorption spectroscopy provides a sensitive probe of local electronic structure and hierarchical organization of bone.

Electronic structure of bone tissue is examined in the frameworks of (i) the modern morphological models of structural and functional organization of the skeleton

in the normal and pathological conditions and (ii) the quantum-mechanical 3DSL model describing propagation of electronic waves in a three-dimensional superperiodic lattice of "black-nanocrystallites-in-muddy-waters". The distinct *HAP-to-bone* red shifts of Ca 2*p*-, P 2*p*- and O 1*s*-to-valence transitions are revealed and attributed to the hierarchy-induced effects. Their origin is discussed rather in details.

The link of the detected spectral shifts with the hierarchical organization of bone tissue is supported. The hierarchy effect on energy of core-to-valence transitions is regarded as a promising tool for medical imaging and nanodiagnostics of bone tissue.

Author contribution statement

All authors are contributed equally to the paper.

References

1. B. Yucesoy, L.E. Charles, B. Baker, C.M. Burchfiel, Work **50**, 261273 (2015)
2. W.F. Neuman, M.W. Neuman, *The chemical dynamics of bone mineral* (University of Chicago Press, Chicago, 1958)
3. J. Currey, *The mechanical adaptation of bones* (Princeton University Press, Princeton, NJ, 1984), p. 294
4. S. Weiner, H.D. Wagner, Annu. Rev. Mater. Sci. **28**, 271 (1998)
5. Yu.I. Denisov-Nikolski, S.P. Mironov, N.P. Omeljanenko, I.V. Matveichuk, *Actual problems of theoretical and clinical osteoartrology* (Novosti, Moscow, 2005), p. 336 [in Rus]
6. B.A. Zhilkin, Yu.I. Denisov-Nikolski, A.A. Doktorov, Uspekhi sovremennoy biologii [Adv. Mod. Biol.] **123**, 590 (2003)
7. A.S. Avrunin, R.M. Tihilov, I.I. Shubniakov, L.A. Parshin, B.E. Melnikov, D.G. Pliev, Morfologiia [Morphology] **6**, 69 (2010)
8. A.S. Avrunin, R.M. Tikhilov, A.B. Abolin, I.G. Shcherbak, Morphology **127**, 78 (2005)
9. M. Buehler, Nanotechnology **18**, 295102 (2007)
10. C.-K. Loong, C. Rey, L.T. Kuhn, C. Combes, Y. Wu, S.-H. Chen, M.J. Glimch, Bone **26**, 599 (2000)
11. M.J. Olszta, D.J. Odom, E.P. Douglas, L.B. Gower, Connect. Tissue Res. **44**, 326334 (2003)
12. J.D. Pasteris, C.H. Yoder, B. Wopenka, Am. Mineral. **99**, 16 (2014)
13. C. Rey, J.L. Miquel, L. Facchini, A.P. Legrand, M.J. Glimcher, Bone **16**, 583 (1995)
14. A.S. Avrunin, R.M. Tihilov, L.K. Parshin, I.I. Shubniakov, Traumatol. Orthop. Russ. **2**, 77 (2008)
15. A.A. Pavlychev, A.S. Avrunin, A.S. Vinogradov, E.O. Filatova, A.A. Doctorov, Yu.S. Krivosenko, D.O. Samoilenko, G.I. Svirskiy, A.S. Konashuk, D.A. Rostov, Nanotechnology **27**, 504002-1 (2016)
16. A. Gautieri, S. Vicentini, A. Redaelli, M. Buehler, Nano Lett. **11**, 757 (2011)
17. P. Rulis, L. Ouyang, W.Y. Ching, Phys. Rev. **70**, 155104 (2004)
18. K. Matsunaga, A. Kuwabara, Phys. Rev. B **75**, 014102 (2007)
19. A.S. Avrunin, Yu.I. Denisov-Nikolsky, A.A. Doktorov, Yu.S. Krivosenko, D.O. Samoilenko, A.A. Pavlychev, I.I. Shubniakov, Traumatol. Orthop. Russ. **3**, 37 (2015)
20. R. Legros, N. Balmain, G. Bonel, Calcif. Tissue Int. **41**, 13744 (1987)
21. S. Bertazzo, C.A. Bertran, J.A. Camilli, Key Eng. Mater. **309–311**, 11 (2006)
22. B. Wopenka, J.D. Pasteris, Mater. Sci. Eng. C **25**, 131 (2005)
23. O. Frank-Kamenetskaya, A. Koltsov, M. Kuzmina, M. Zorina, L. Poritskaya, J. Mol. Struct. **992**, 9 (2011)
24. C. Chadefaux, C. Vignaud, E. Chalmin, J. Robles-Camacho, J. Arroyo-Cabrales, E. Johnson, I. Reiche, Am. Mineral. **94**, 27 (2009)
25. V. Heine, Solid State Phys.: Adv. Res. Appl. **24**, 1 (1970)
26. X.O. Brykalova, D.A. Rostov, Yu.S. Krivosenko, A.A. Pavlychev, J. Electron. Spectrosc. Related. Phenom. **196**, 71 (2014)
27. W. Tong, M.J. Glimcher, J.L. Katz, L. Kuhn, S.J. Eppell, Calcif. Tissue Int. **72**, 592 (2003)
28. A.J. Taylor, E. Rendina, B.J. Smith, D.H. Zhou, Chem. Phys. Lett. **588**, 124 (2003)
29. A.S. Avrunin, A.A. Pavlychev, A.A. Doktorov, A.S. Vinogradov, D.O. Samoilenko, G.I. Svirskiy, Traumatol. Orthop. Russ. **22**, 88 (2016)
30. J. Rajendran, S. Gialanella, P.B. Aswath, Mater. Sci. Eng. C **33**, 3968 (2013)
31. A. Nikolaev, V.V. Bazhenov, O.V. Frank-Kamenetskaya, O.V. Petrova, in *Extreme Biomimetics*, edited by H. Ehrlich (Springer, 2017)
32. E.F. Aziz, N. Ottosson, M. Faubel, I.V. Hertel, B. Winter, Nature **455**, 89 (2008)
33. C.D. Cappa, J.D. Smith, B.M. Messer, R.C. Cohen, R.J. Saykally, J. Phys. Chem. B **110**, 5301 (2006)